

| | | |
|------|------------------|------|
| MAST | PROJECT 1: WAVES | G8-M |
|------|------------------|------|

Comparison of computations with Boussinesq-like models and laboratory measurements

M.W. Dingemans

H1684.12

April 9, 1994

| | | |
|----------|------------------------------------------------------|-----------|
| 1 | Introduction | 1 |
| 2 | The measurements | 4 |
| 3 | The mathematical models | 5 |
| 3.1 | Danish Hydraulic Institute (DHI) | 6 |
| 3.2 | Delft Hydraulics (WL) | 8 |
| 3.3 | Aristotle University of Thessaloniki (AUT) | 9 |
| 3.4 | LEGI-IMG Grenoble | 10 |
| 3.5 | Snamprogetti (Snam) | 11 |
| 3.6 | University of Groningen (UG) | 11 |
| 4 | Comparison of computations with measurements | 12 |
| 4.1 | Measurement condition A | 12 |
| 4.1.1 | DHI results | 12 |
| 4.1.2 | Delft Hydraulics and University of Groningen results | 14 |
| 4.1.3 | A Hamiltonian and a Boundary element model | 14 |
| 4.1.4 | Legi results | 16 |
| 4.1.5 | Snamprogettiti results | 17 |
| 4.1.6 | University of Thessaloniki results | 18 |
| 4.2 | Measuring condition B | 18 |
| 4.3 | Measuring condition C | 20 |
| 5 | Discussion and recommendations | 20 |

In this note results of the comparison between computation of Boussinesq-like models and measurements in a wave flume is given. Purpose of the exercise is to enhance the usability of the models of the various institutes.

1. Introduction.

It is already known for a long time that one of the major discrepancies between computations with Boussinesq-like models and measurements, is due to the inaccurate representation of the linear frequency dispersion in the Boussinesq-like long

wave models. A comparison of various models as given in Dingemans (1973) showed already large differences between the frequency dispersion of various models. A comparison with measurements in a flume (Dingemans, 1976) showed that the computed wave profiles were also found in the measurements, but at a different location. This was ascribed to the inaccurate frequency dispersion.

Recently Madsen et al. (1991) took up a suggestion of Witting (1984) and suggested a form of Boussinesq-like equations with a much improved frequency dispersion. This is based upon a $[1/1]$ Padé expansion in the expansion parameter $(kh)^2$ of the linear expression for the square of the phase velocity, c^2 , and the corresponding set of differential equations is sought for then. Madsen et al. (1991, 1992) performed this task by adding higher-order terms consisting of third derivatives in t and x to the horizontal momentum equation. As shown in a lecture by Dingemans (1992) at the final Mast-G6M Workshop in Pisa, a somewhat more systematic way by means of operator correspondence gives various possible models, one of which was given by Madsen et al. (1991). (A written account can be found in Dingemans, 1994). A similar approach is given by Mooiman (1991) who considers a Padé approximation of c , yielding a slightly less good agreement as does the approximation of c^2 .

For engineering practice it is highly desirable to be able to treat as short waves as possible, although the Boussinesq approximation is strictly valid only for (fairly) long waves. A Padé expansion of order $[1/1]$ then gives the best possible result without introducing still higher derivatives than the third.

As argued above, deviations between computations and measurements occur for short wave components when these components are freely moving, that is when the components are moving according to their dispersion characteristics. Non-linear waves have the typical characteristic that many components are phase-locked and higher harmonics then travel with the velocity of the basic wave, which velocity is determined by some non-linear correction of the linear dispersion relation. Permanent wave forms are possible when the frequency and amplitude dispersion effects balance each other. An example of a permanent wave form is a cnoidal wave in which all higher harmonics are phase-locked. When such a cnoidal wave progresses up a slope, then occasionally an adiabatic approximation is used to describe the shoaling process and it is assumed that the parameters describing the cnoidal wave are changing slowly, but the wave form remains of cnoidal shape. In such an adiabatic approximation all wave components are therefore supposed to remain phase-locked. In general this is not true. A generation of more higher harmonics gives always both free and locked harmonics. This phenomenon becomes especially apparent when the depth is increasing again so that the difference between the phase velocities of the bound and the free components increases.

Above remarks can be substantiated in the following way. For the decreasing-depth situation the parameter kh also decreases, where k is the wave number of the primary wave. As for long waves the phase velocity in the computational model changes little from the exact linear one, the free waves propagate with a velocity near to the one of the primary wave, and it takes a long distance before differences become visible. On the backward slope the depth is increasing fast and so does the parameter kh . For large values of kh the difference between the computational phase velocity and the exact one increases and the free waves have a velocity which

deviates much more from the one of the basic wave than for the shallower depth. Because of the phase differences between free and locked higher harmonics soon differences in wave profiles between computations and measurements will be visible.

A discriminating test between various models based on Boussinesq-like approximations is then provided by a bar-type geometry. On the upward slope effects of nonlinearity generate higher harmonics and on the downward slope the difference between locked and free modes becomes clearly visible.

A number of flume and basin experiments based on a bar-type geometry for fairly long waves have become available in the past decade. Some measurements of Dingemans (1976) are also available, but in less detail and of a much less discriminating nature (waves on a shelf). In a number of measurements a trapezoidal bar has been taken into consideration, in which the offshore slope is 1 : 20 and the shoreward slope 1 : 10, while the depth in the horizontal depth parts is 40 cm and on the horizontal part of the bar (of extent 2 m) the depth is 10 cm. Such a geometry has been used by Dingemans (1987) in a verification study of the wave propagation model HISWA and by Beji and Battjes in a flume experiment at Delft University of Technology, see Battjes and Beji (1993) and by Liberatore and Petti (1992) in a flume in Padua. Because in Padua no reflection and bound-wave compensation was present in the software which steers the wave generator, some tests are repeated in Florence where such software has recently been installed.

Recently, January 1993, Gert Klopman of Delft Hydraulics has performed three regular wave tests already done by Beji, but with a linear scale of 2, i.e., an undisturbed depth of 80 cm and 20 cm depth above the bar. Care has been exercised to ensure that exactly the same conditions were performed, i.e., also a wave period $T = 2.02\sqrt{2}s$ has been taken. In the experiments of Klopman, performed as part of the LIP program, a number of tests with following and opposing current have been performed and also information about long bound waves is present. The experiments to be used in the present study do have active wave absorption and also compensation for bound long waves. As the boundary conditions of the wave board and the reflection from the beach have been taken care of very accurately, we will use these measurements here. The set-up of the experiments is the same as the one reported in Luth et al. (1994). The layout is given in Figure 1 and the placement of the wave gauges is given in Table 1.

| | | | | | | |
|---------|------|------|-------|-------|-------|-------|
| meas 01 | 3.04 | 9.44 | 20.04 | 26.04 | 30.44 | 37.04 |
| meas 02 | 7.04 | 9.44 | 24.04 | 28.04 | 33.64 | 41.04 |

TABLE 1

The location of the wave height gauges of the LIP experiments

For the measurements we use the linear scale factor of 2 so that the results are directly comparable to the measurements of Battjes and Beji and also to the various computations.

We consider the geometry as given in Figure 2. It is noted that the distance from the mean position of the wave maker to the toe of the bar (6 m) is, scaled, different from the corresponding distance in the LIP experiment. This is estimated to be not significant. The location of the wave gauges corresponds in the two experimental set-ups when the distances are measured from the start of the crest of the bar. Also

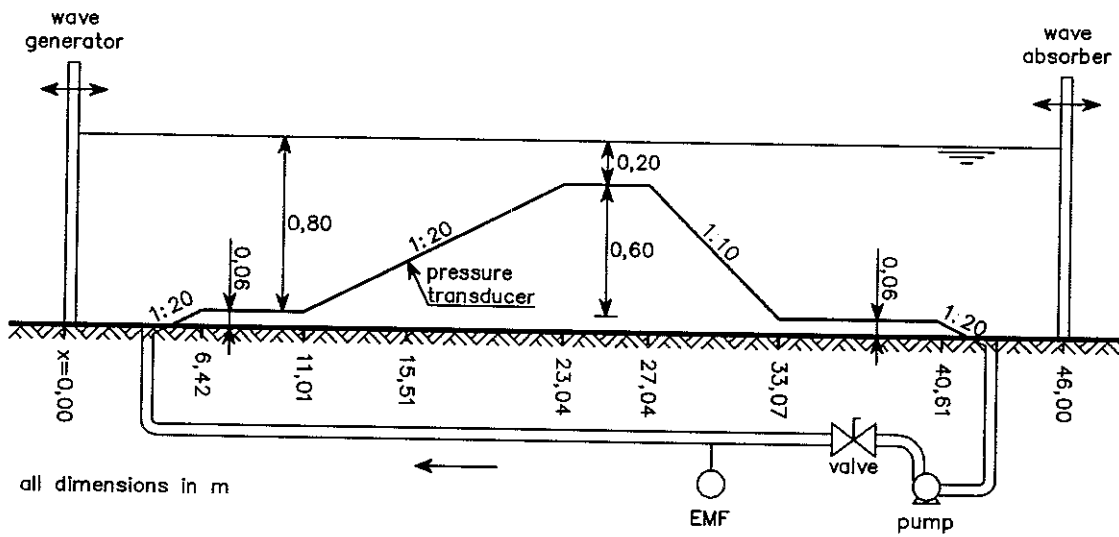


FIG 1. The layout of the LIP experiment.

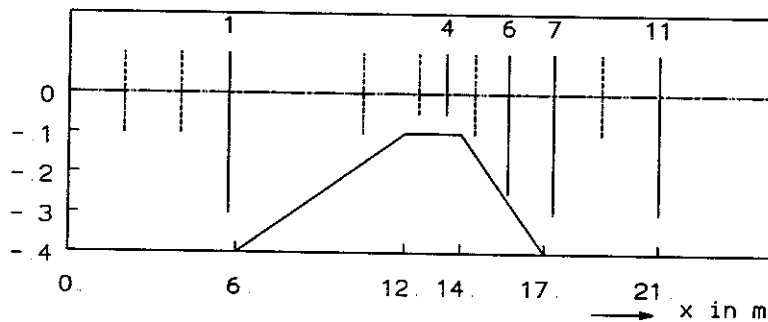


FIG 2. The bottom geometry and the location of the wave gauges.

the slight change in water depth (from 86 to 80 cm) as needed in the LIP experiment for the generation of current is estimated to be of no importance.

2. The measurements.

In the measurements of Beji seven wave gauges have been used, numbered 1 to 7. Some of these are depicted in Figure 2. For the computations it has been decided that surface elevations at more stations was advisable to be able to follow the evolution of wave profiles more easily. The stations 8 to 12 have been added for that purpose. In Table 2 the stations and their locations have been given. Except for the station at 23 m surface elevations have been measured at all stations in the Delft Hydraulic measurements. To be able to do this, wave gauges had to be replaced and the experiment had to be repeated once. As a check, wave gauge 1 has kept fixed so that a check on the repeatability of the experiment is possible. The location of the measuring probes has also been indicated in Figure 2. Here distinction is made between the stations primarily used in the following discussion and the other stations.

The measurements in the flume of Delft Hydraulics had a linear scale of 2 compared to the measurements of Beji at the Delft University of Technology, i.e., an initial depth of 80 cm was used, etc. In the present discussion we rescaled everything to the geometry used by Beji. The measurements of Delft Hydraulics are used in this study. The values of the measurements and the location of the wave gauges are always given in scaled quantities (i.e. belonging to an initial depth of 0.40 m) unless

| station | location | Delft Hydr. | Beji | remarks |
|---------|----------|-------------|------|--------------------------------------|
| 1 | 5.70 | + | + | providing the boundary condition |
| 2 | 10.50 | + | + | on upward slope |
| 3 | 12.50 | + | + | on the bar |
| 4 | 13.50 | + | + | on the bar |
| 5 | 14.50 | + | + | on downward slope |
| 6 | 15.70 | + | + | on downward slope |
| 7 | 17.30 | + | + | just behind the bar |
| 8 | 2.00 | + | - | close to wave maker |
| 9 | 4.00 | + | - | |
| 10 | 19.00 | + | - | further behind the bar |
| 11 | 21.00 | + | - | far behind the bar |
| 12 | 23.00 | - | - | no measurement because lack of space |

TABLE 2
Location of wave measuring stations.

stated otherwise explicitly.

Three measuring conditions are considered, conditions A, B and C:

A $T = 2.02$ s and $H = 2$ cm non-breaking waves

B $T = 2.525$ s and $H = 2.9$ cm spilling breakers between 13.3 and 15.3 m

C $T = 1.01$ s and $H = 4.1$ cm non-breaking waves

We first consider the measuring condition A. A view of the surface elevation in the time window from 10 to 70 s of unscaled time is given in Figure 3. Here the two measuring sets are denoted by bea01 and bea02 respectively¹. Free surface elevations at the various wave gauges for condition A are given in the right of Figure 3. These surface elevations are used for comparison with computed free surface elevation profiles.

Measured free surface elevations for measuring condition B are given in Fig. 4. Because in the measurement of the first series (beb01) a rather long stretch with no signal was present, we selected for beb01 the time window between 20 and 80 s, while for the second series beb02 is taken the window between 10 and 70 s. The values on the time-axis have been given only for the lowest Figures, the elevations taken at 13.5 and 21 m. As can be seen from the left part of Fig. 4, these elevations come from different series of measurements. In measurement B spilling breakers have been observed in the region between 13.3 and 15.3 m (scaled, which corresponds to between 26 and 29 m unscaled). Behind the bar cross waves were present. This is why the measurement at 21 m is so different from the one at 19 m.

In the same way the free surface elevations as obtained from measurement condition C are given in Figure 5. Notice that left for measuring station 13.5 m near 70 s some increase is seen in the wave amplitude. Further investigation, by plotting the surface elevation up to 140 s, shows that this increase is due to a modulation in the signal.

3. The mathematical models.

¹ The names of the files of the measurements performed by delft hydraulics are explicitly given because the measurements are available to the participants after completion of this report

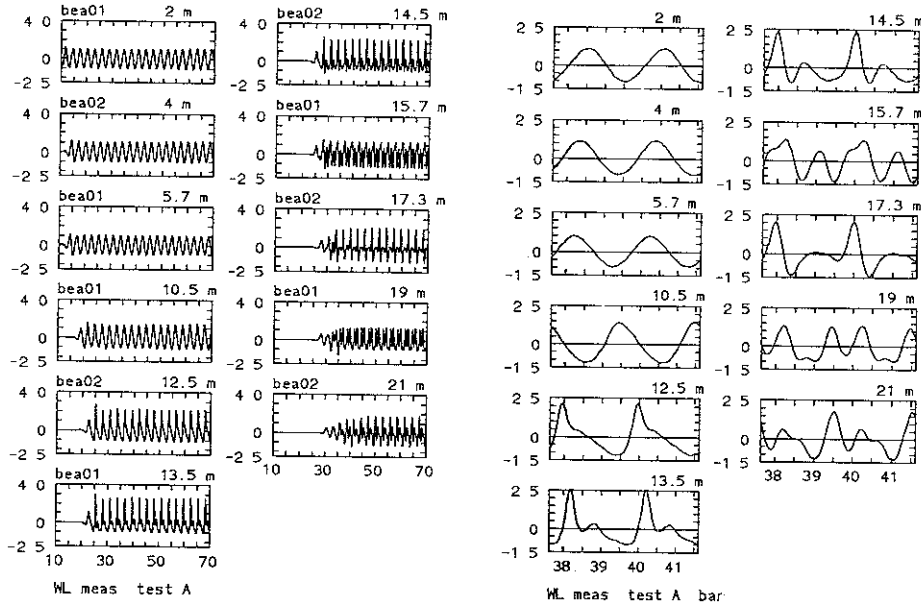


FIG 3. WL measurements in the Schelde flume for condition A. Left a time window of 60 s is shown, with unscaled time; right a time window of 5 s with scaled time is shown.

Computations have been performed with various Boussinesq-type models of institutes participating in Project 1 of Mast G8-M. These models are described briefly in this section.

3.1. Danish Hydraulic Institute (DHI).

The Boussinesq-type model of DHI which has been used here is described in Madsen et al. (1991, 1992) is valid for small bottom slopes and reads

$$\begin{aligned}
 \frac{\partial q}{\partial t} + \frac{\partial}{\partial x} \left(\frac{q^2}{h + \zeta} \right) + g(h + \zeta) \frac{\partial \zeta}{\partial x} &= (1 + 3b) h^2 \frac{\partial^3 q}{\partial t \partial x^2} + b g h^3 \frac{\partial^3 \zeta}{\partial x^3} + \\
 &+ h h_x \left[\frac{1}{3} \frac{\partial^2 q}{\partial t \partial x} + 2 b g h \frac{\partial^2 \zeta}{\partial x^2} \right]
 \end{aligned}
 \tag{1}$$

$$\frac{\partial \zeta}{\partial t} + \frac{\partial q}{\partial x} = 0$$

where the flux q is given by

$$u(x, t) = \frac{q(x, t)}{h(x) + \zeta(x, t)}
 \tag{2}$$

This model for small bottom slopes might be a reduction of a model valid for larger bottom slopes² as has been given by Dingemans (1994):

$$\begin{aligned}
 \frac{\partial q}{\partial t} + \frac{\partial}{\partial x} \left(\frac{q^2}{h + \zeta} \right) + g(h + \zeta) \frac{\partial \zeta}{\partial x} &= b g h^2 \frac{\partial^2}{\partial x^2} \left(h \frac{\partial \zeta}{\partial x} \right) + \\
 &+ h^2 \frac{\partial}{\partial t} \left[\left(\frac{1}{2} + b \right) \frac{\partial^2 q}{\partial x^2} - \frac{1}{6} h \frac{\partial^2}{\partial x^2} \left(\frac{q}{h} \right) \right]
 \end{aligned}
 \tag{3}$$

$$\frac{\partial \zeta}{\partial t} + \frac{\partial q}{\partial x} = 0$$

² Many possibilities exist for the larger bottom slope models. The presented one is just one of them.

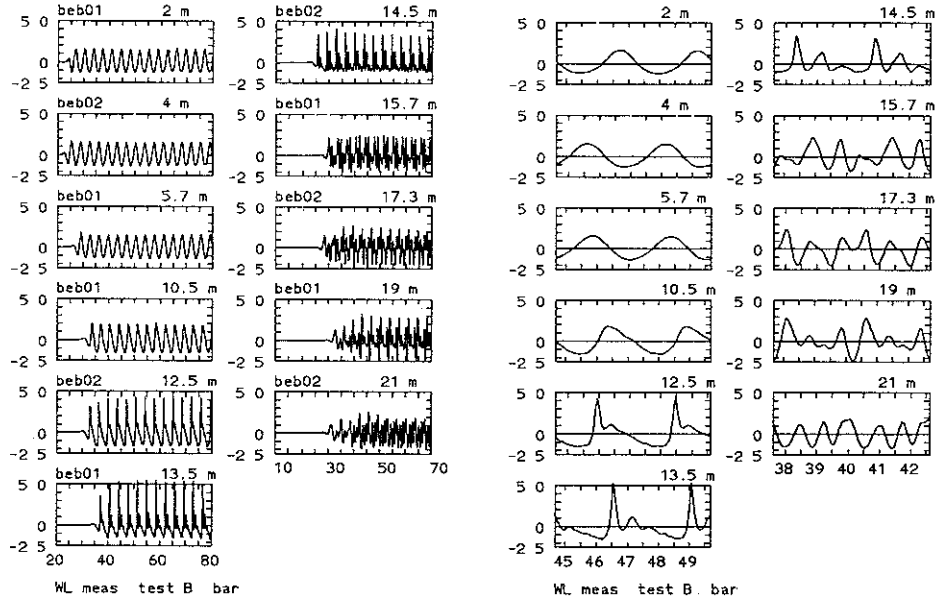


FIG. 4. WL measurements in the Schelde flume for condition B. Left a time window of 60 s is shown, with unscaled time; right a time window of 4 s with scaled time is shown.

The corresponding set of equations in the averaged velocity u is given by

$$\begin{aligned}
 (4) \quad \frac{\partial u}{\partial t} + u \frac{\partial u}{\partial x} + g \frac{\partial \zeta}{\partial x} &= bgh \frac{\partial^2}{\partial x^2} \left(h \frac{\partial \zeta}{\partial x} \right) + \\
 &+ h \frac{\partial}{\partial t} \left[\left(\frac{1}{2} + b \right) \frac{\partial^2 hu}{\partial x^2} - \frac{1}{6} h \frac{\partial^2 u}{\partial x^2} \right] \\
 \frac{\partial \zeta}{\partial t} + \frac{\partial}{\partial x} [(h + \zeta) u] &= 0
 \end{aligned}$$

where b is a parameter which is used to obtain a better correspondence of the dispersion relation with the exact one for linear waves. For a Padé expansion of c^2 one obtains $b = 1/15$. The dispersion relation of the sets (1), (3) and (4) reads

$$(5) \quad \frac{c^2}{gh} = \frac{1 + b(kh)^2}{1 + \left(\frac{1}{3} + b\right)(kh)^2}.$$

For $b = 0$ one obtains the Boussinesq-type model usually obtained for the velocity variable which is the over the instantaneous depth averaged one:

$$\begin{aligned}
 (6) \quad \frac{\partial u}{\partial t} + u \frac{\partial u}{\partial x} + g \frac{\partial \zeta}{\partial x} &= \frac{1}{2} \frac{\partial}{\partial t} \left[h \frac{\partial^2 (hu)}{\partial x^2} - \frac{1}{3} h^2 \frac{\partial^2 u}{\partial x^2} \right] \\
 \frac{\partial \zeta}{\partial t} + \frac{\partial}{\partial x} [(h + \zeta) u] &= 0
 \end{aligned}$$

The computational phase velocity c as resulting from (5) is now compared to the exact linear one given by

$$(7) \quad \frac{c}{\sqrt{gh}} = \sqrt{\frac{\tanh kh}{kh}},$$

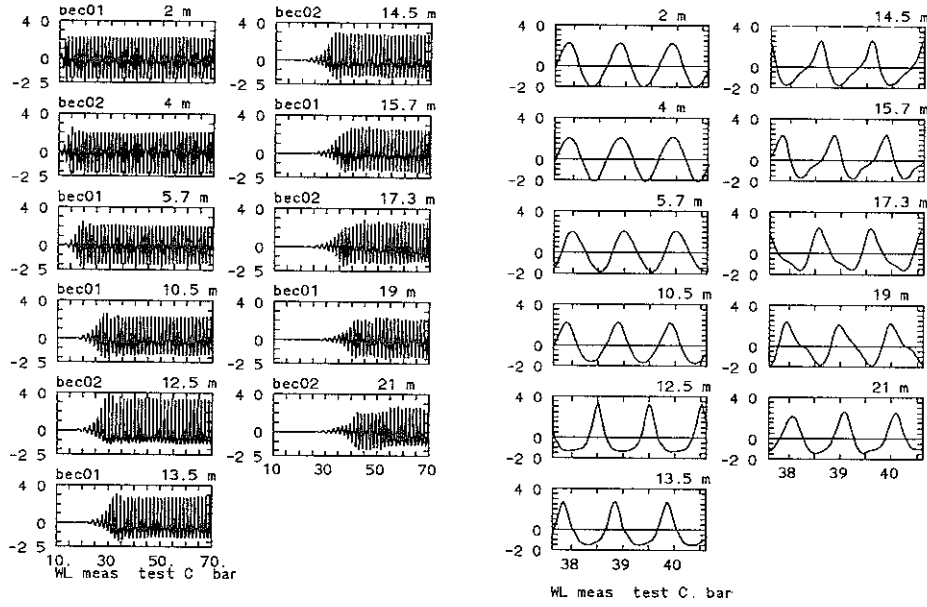


FIG. 5 WL measurements in the Schelde flume for condition B. Left a time window of 60 s is shown, with unscaled time; right a time window of 4 s with scaled time is shown

where the cases $b = 1/15$ and $b = 0$ are considered. Later also a phase velocity which is the $[1/1]$ Padé expansion of c appears. This velocity is given by

$$(8) \quad \frac{c}{\sqrt{gh}} = \frac{1 + \frac{9}{60}(kh)^2}{1 + \frac{19}{60}(kh)^2}$$

The different velocities, scaled with \sqrt{gh} are shown in Figure 6 as function of kh . Here we gave a large range up to $kh = 10$ but it should be noted that the important part lies near $kh = 2$

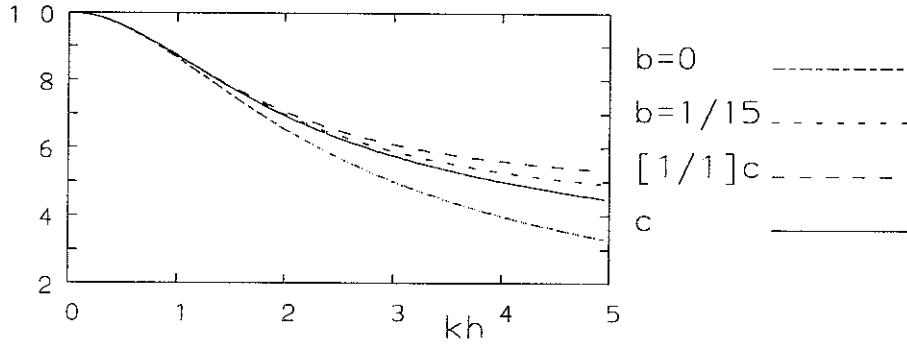


FIG. 6. Computational and exact celerities compared

In order to see the differences clear, we also give a Figure with the relative differences as a percentage. Here $(c_c - c_e)/c_e$ is given where c_c is one of the computational velocities (5) and (8) and c_e is the exact linear celerity given by (7).

3.2. Delft Hydraulics (WL).

The Boussinesq-type model used by Delft Hydraulics is an approximate Hamiltonian model with frequency behaviour which corresponds with a Padé expansion of the phase velocity c , see Mooiman (1991). The model reads:

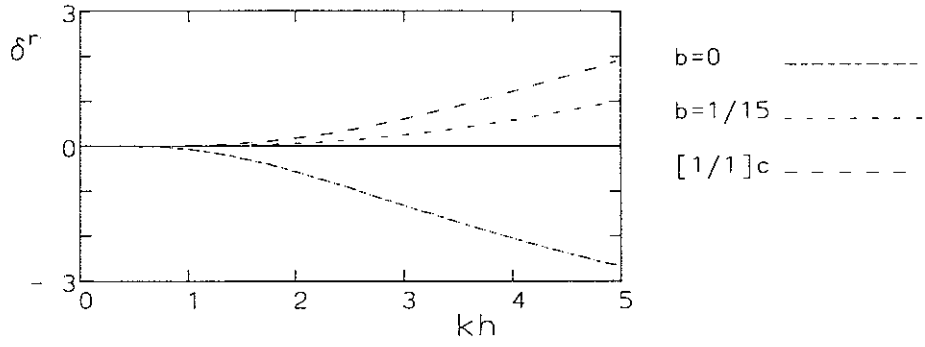


FIG. 7. Deviations between computational and exact celerities.

$$(9) \quad \begin{aligned} \frac{\partial u}{\partial t} &= -\mathcal{G}_a(u) \frac{\partial}{\partial x} \{ \mathcal{G}_a(u) \} - g \frac{\partial \zeta}{\partial x} \\ \frac{\partial \zeta}{\partial t} &= -\frac{\partial}{\partial x} \{ \mathcal{G}_a [(h + \zeta) \mathcal{G}_a(u)] \}, \end{aligned}$$

with $\mathcal{G}_a = \mathcal{Q}_\beta^{-1} \mathcal{Q}_\alpha$ and

$$(10) \quad \mathcal{Q}_\gamma = 1 - \frac{1}{4} h \frac{\partial^2}{\partial x^2} h + \frac{1}{12} \gamma \frac{\partial}{\partial x} \left(h^2 \frac{\partial}{\partial x} \right), \quad \gamma = \alpha \text{ or } \beta.$$

The symbol of \mathcal{G}_a (i.e., the Fourier transform of the operator \mathcal{G}_a) is given as

$$(11) \quad \hat{G}_a = \frac{1 + \frac{1}{6} \alpha (kh)^2}{1 + \frac{1}{6} \beta (kh)^2},$$

with $\alpha = 9/10$ and $\beta = 19/10$. For the present model we have $c/\sqrt{gh} = \hat{G}_a$, see also Eq. (8).

3.3. Aristotle University of Thessaloniki (AUT).

At AUT Karambas has derived Boussinesq-type equations with improved frequency dispersion which read for a horizontal bottom as follows:

$$(12) \quad \begin{aligned} \frac{\partial u}{\partial t} + u \frac{\partial u}{\partial x} + g \frac{\partial \zeta}{\partial x} &= h^2 A \frac{\partial^3 u}{\partial x^2 \partial t} \\ \frac{\partial \zeta}{\partial t} + \frac{\partial}{\partial x} [(h + \zeta) u] &= 0 \end{aligned}$$

with dispersion relation

$$(13) \quad \frac{c^2}{gh} = \frac{1}{1 + A (kh)^2}.$$

Comparison with the dispersion relation (5) shows that the relation between b and A is given by

$$(14) \quad A = \frac{1}{3 (1 + b (kh)^2)} \quad \text{and} \quad b = \frac{1 - 3A}{3A (kh)^2}$$

For $A = 1/3$ the model (6) is recovered. The particular value of A which is to be applied follows for a value of kh from

$$(15) \quad A = \frac{1}{\sinh kh} \sum_{n=0}^{\infty} \frac{1}{2n+3} \frac{(kh)^{2n+1}}{(2n+1)!}.$$

Of course, the problem of which value of kh to use in a area with changing depth remains. Furthermore, even with constant depth, the choice of kh signifies that effectively only waves with a fixed frequency may be computed, and, moreover, the generation of higher harmonics poses a problem in this respect especially the free harmonics which are seen to be generated on the backside of the bar in the present measurements effectively invalidates the model

3.4. LEGI-IMG Grenoble.

Barthélemy and Guibourg of the LEGI-IMG has used a Serre model with improved frequency dispersion of the following form:

$$(16) \quad \begin{aligned} \frac{\partial q}{\partial t} + \frac{\partial F}{\partial x} &= \nu \frac{\partial^2 u}{\partial x^2} \\ \frac{\partial \zeta}{\partial t} + \frac{\partial}{\partial x} [(h + \zeta) u] &= 0 \end{aligned}$$

where

$$(17) \quad \begin{aligned} F = uq - \frac{1}{2}u^2 + g(h + \zeta) - \frac{1}{2}(h + \zeta)^2 \left(\frac{\partial u}{\partial x} \right)^2 + \frac{1}{2}u^2 h_x^2 + \\ + (h + \zeta) h_x u \frac{\partial u}{\partial x} + B \left(h^2 u \frac{\partial^2 u}{\partial x^2} - gh^2 h_{xx} - 2gh h_x h_{xx} \right) \end{aligned}$$

$$(18) \quad q = u(1 + \Omega) - \frac{1}{3(h + \zeta)} \frac{\partial}{\partial x} \left[(h + \zeta)^3 \frac{\partial u}{\partial x} \right] - Bh^2 \frac{\partial^2 u}{\partial x^2}$$

$$(19) \quad \Omega = h_x \frac{\partial}{\partial x} (h + \zeta) + \frac{1}{2} (h + \zeta) h_{xx} + h_x^2.$$

and ν is the kinematic viscosity. In first instance computations with viscosity have been performed. A comparison with the measurements showed that the decrease in wave height was much too high. A new set of computations has therefore been carried out in which no effect of viscosity was accounted for. The computations of LEGI are performed with $B = 1/20$. The numerical scheme used is the one of Su and Mirie (1980). It is an implicit finite-difference scheme with a predictor-corrector algorithm.

The parameter B has been introduced to obtain good frequency-dispersion behaviour. Therefore it is quite uncommon that B also multiplies a non-linear term in the expression for F . Also terms solely expressed in the still-water depth h and its spatial derivatives, without multiplication with either u or ζ occur in F . Moreover, these depth-terms are multiplied by the parameter B . For linear waves and horizontal bottom the equation system becomes

$$\begin{aligned} \frac{\partial u}{\partial t} + g \frac{\partial \zeta}{\partial x} &= \left(B + \frac{1}{3} \right) h^2 \frac{\partial^3 u}{\partial t \partial x^2} \\ \frac{\partial q}{\partial t} + h \frac{\partial u}{\partial x} &= 0, \end{aligned}$$

which set has the dispersion relation

$$\frac{c^2}{gh} = \frac{1}{1 + (B + (kh)^2)} = \frac{1}{1 + (B + \frac{1}{3})(kh)^2}$$

and which is not a Padé expansion of the square of the exact linear phase velocity. In order to achieve that with the given first equation of above set it is necessary to have the extra term $Bh^3 u_{xx}$ in the right-hand side of the second equation of above set, see Dingemans (1994), section 5.5.2. A simple change of u into q in the continuity equation does not provide the wanted result.

3.5. Snamprogetti (Snam).

Brocchini of Snamprogetti performed computations with both a Boussinesq-type model and a Serre-type model. The Boussinesq-type model is the same as given in (6) and the Serre-type model reads as follows.

$$\begin{aligned} u_t + uu_x + g\zeta_x &= hh_x u_{xt} + \frac{h^2}{3} u_{xxt} + h\zeta_x u_{xt} + \frac{2}{3} h\zeta u_{xxt} + \frac{h^2}{3} \frac{\partial}{\partial x} (uu_x - (u_x)^2) \\ (20) \quad \zeta_t + [(h + \zeta) u]_x &= 0. \end{aligned}$$

3.6. University of Groningen (UG).

Recently Van Veen and Wubs (1993) proposed a different Hamiltonian Boussinesq-type of model. The advantage of this model over that of mooiman is a reduction in computer time with a factor 2 because two instead of four Helmholtz-type of problems have to be solved for the complicated operator. The model reads

$$\begin{aligned} (21) \quad \frac{\partial \mathbf{u}}{\partial t} &= -\frac{1}{\beta} (\mathcal{P} \mathbf{u} \cdot \nabla) \mathcal{P} \mathbf{u} - \frac{\alpha}{\beta} (\mathbf{u} \cdot \nabla) \mathbf{u} - g \nabla \zeta \\ \frac{\partial \zeta}{\partial t} &= -\frac{1}{\beta} \nabla \cdot [(h + \zeta) \mathcal{P} \mathbf{u}] - \frac{\alpha}{\beta} \nabla \cdot [(h + \zeta) \mathbf{u}]. \end{aligned}$$

where the operator \mathcal{P} is given by

$$(22) \quad \mathcal{P} = (h + \zeta)^{-1} \left((h + \zeta)^{-1} + \beta \mathcal{A} \right)^{-1}$$

with \mathcal{A} given by

$$(23) \quad \mathcal{A}f = -\frac{1}{6} h \nabla^2 f + \nabla^2 (hf) + \frac{1}{3h} |\nabla h|^2 f,$$

with f some well-behaved function. The parameters α and β are determined such that a Padé expansion of the phase velocity c is obtained. we have

$$(24) \quad c^2 \cong \frac{1 + \frac{1}{3}\alpha (kh)^2}{1 + \frac{1}{3}\beta (kh)^2}$$

so that we have $\alpha = 1/5$ and $\beta = 6/5$.

4. Comparison of computations with measurements.

With most of the numerical models discussed here computations for all three measurements have been provided. We give results of all models for test A, but give only a few results for tests B and C. It turned out that test A was of such a discriminating nature that effectively the accuracy of all models could be judged from that case alone. As the frequency dispersion proved to be of paramount importance, also for tests B and C results are shown for non-optimal frequency dispersion (i.e., $b = 0$) for both Boussinesq and Serre-type models. These results have been obtained with the DHI and Legi models.

4.1. Measurement condition A.

A comparison between computations and measurements can be carried out in a number of ways. Whichever method is chosen, a graphical comparison is needed. Nearly all computations have been performed for a duration of 40 s, which is enough so that permanent wave profiles are obtained at the farthest stations. Over 23 m we have an average depth of 29.8 cm and thus, based on $c = \sqrt{gh}$ a mean celerity $c = 1.71$ m/s so that it takes 13.46 s for the main wave to travel the distance of 23 m. So much reserve is present that the free higher harmonics of interest have certainly reached the farthest station.

For test A we have $T\sqrt{g/h} = 10.0$, so the basic wave is well in the long wave region (which may be loosely defined as $T\sqrt{g/h} > 7$).

The test case A is such that on the horizontal bottom not much happens. This has been checked by a computation with the Delft Hydraulics model (see Dingemans, 1994, section 5.9). Higher bound harmonic components are generated on the first slope and the shallow part is so short, while the local non-linearity is large, that not much phase difference between the free and the bound harmonics is developed here. On the second (downward) slope the depth increases rather fast and there the difference in celerity between the higher harmonic bound and free waves increases fast. It is here where the difference between the various numerical models manifests itself clearly. The wave form changes much in this second slope region. This is clear from the measurements as given in Figure 3.

We plot all computed profiles in the same way as the measurements are plotted in Figure 3. By inspection of the computations with all models considered it follows that all models performed good up to the station at 13.5 m. Notice that this station lies on top of the bar (which extends from 12 to 14 m). That this good correspondence is true is shown on the two sets of equations of DHI, one with improved frequency dispersion ($b = 1/15$) and one without it ($b = 0$).

4.1.1. DHI results.

Results with the DHI models for both improved frequency dispersion ($b = 1/15$) and the usual case ($b = 0$) have been given for all stations in Figure 8.

That the result of both computations is indeed the same up to 13.5 m, is shown in Figure 9 where the results of both computations for 13.5 m have been plotted together. The correspondence between the computation and the measurement is shown in the right-hand part of Figure 9.

Beyond 13.5 m the results from both computations show markedly increasing differences. In order to facilitate the comparison with measurements, we plot all profiles for the computation and the measurement for a duration of about 4 s next

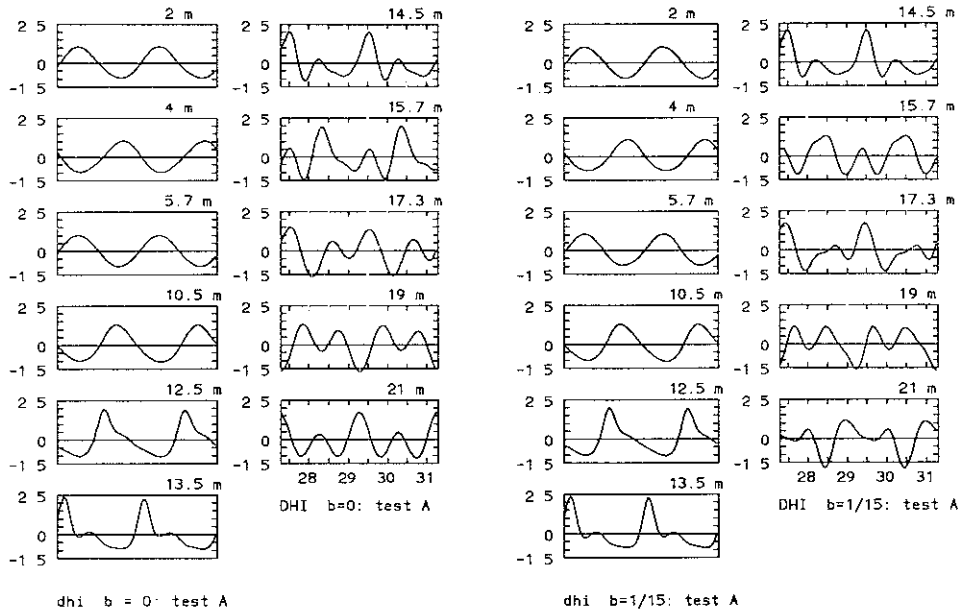


FIG. 8 DHI, $b = 0$ (left) and $b = 1/15$ (right), case A

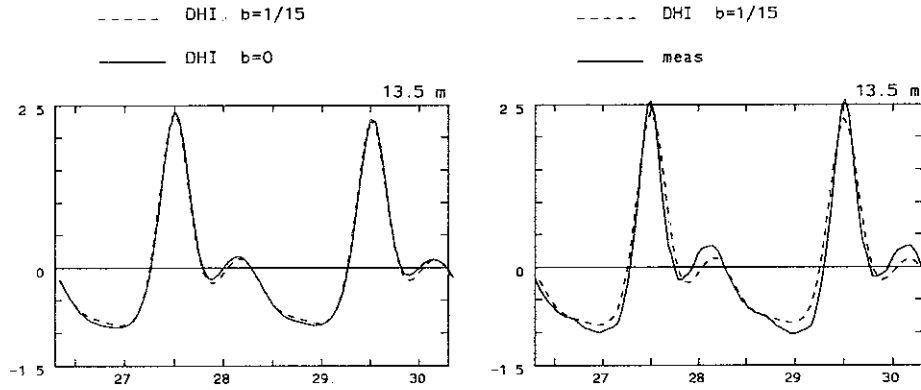


FIG. 9. Computations with DHI model. Left: $b = 0$ and $b = 1/15$ at station 13.5 m for case A. Right: $b = 1/15$, with measurement at $x = 13.5$ m.

to each other. From these Figures it becomes immediately clear whether a model performs good or not. For the DHI model with $b = 1/15$ it is clear from Figure 10 that the computations and the measurements compare well up to 17.3 m. This is stressed in Figures 11 and where the wave profiles of the computation and measurement at locations 15.7 m and 17.3 m have been plotted together.

At 21 m no good correspondence of the computed and measured wave profile is found any more. This is also clear when the two profiles are plotted over each other, see Figure 12. In a Boussinesq-type wave propagation model the dispersion relation is necessarily approximated compared to the exact linear one. Even for a good approximation, eventually, after some distance, the (small) deviations between the phase velocities of the computational model and the exact linear one gives a cumulative effect in that the phases of the various free components differ much and the components even may become 180° out of phase. The distance over which this happens is much longer for an accurate approximation than for a less accurate approximation. But over large distances, when components have become free, the adage that *Boussinesq gives the correct profile at the wrong location* remains true

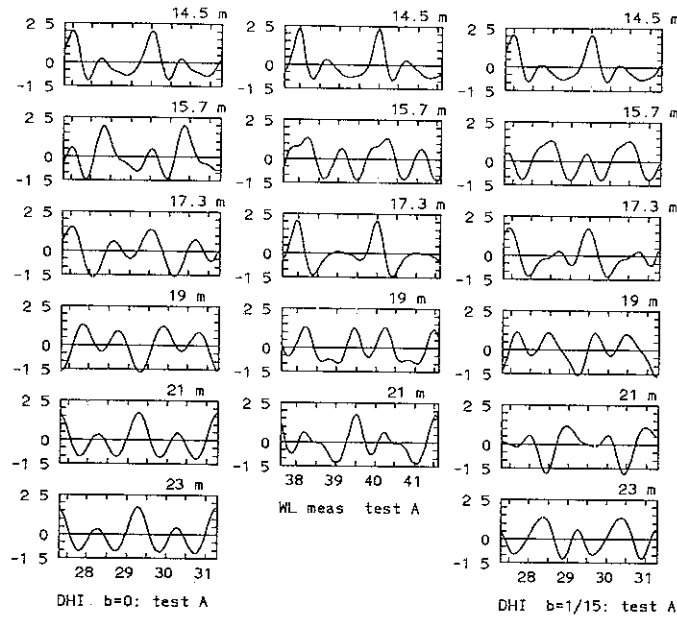


FIG. 10 Measurements and DHI, $b = 0$, and $b = 1/15$, case A.

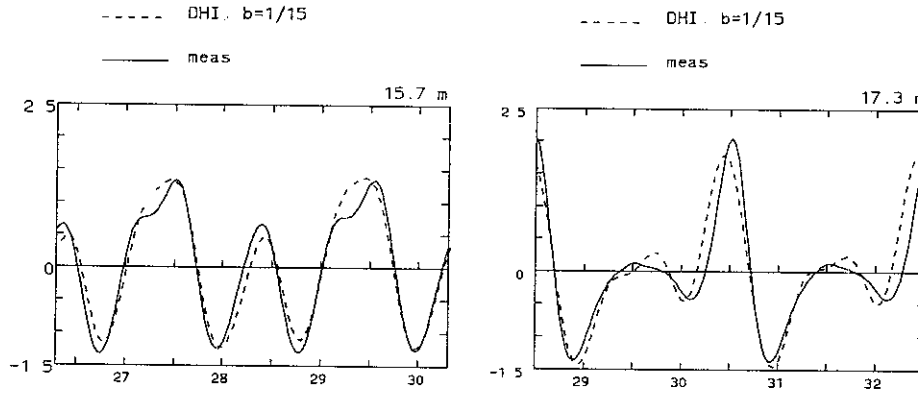


FIG. 11 Comparison DHI, $b = 1/15$, with measurement at $x = 15.7$ m, and at $x = 17.3$ m, case A

4.1.2. Delft Hydraulics and University of Groningen results.

The results obtained with the Boussinesq programs of Delft Hydraulics and University of Groningen are given in Figure 13 for the stations from 14.5 m onwards. In describing these results it should be remembered that the University of Groningen model has a phase velocity which stems from a $[1/1]$ Padé expansion of c^2 , while the Delft Hydraulics model has a phase velocity which is equal to a $[1/1]$ Padé expansion of c . The latter one is somewhat less accurate than the first one as is shown in Figures 6 and 7.

The results shown in Figure 13 show that the University of Groningen model is more accurate than the Delft Hydraulics one. This can be explained from the more accurate dispersion relation of the Groningen model. The DHI result for $b = 1/15$ seems to be somewhat closer to the measurements than either of these two Boussinesq models based on a Hamiltonian approximation method. This is especially clear when considering the results for the station at 17.3 m.

4.1.3. A Hamiltonian and a Boundary element model.

A Hamiltonian model for waves in which the long-wave assumption has not been

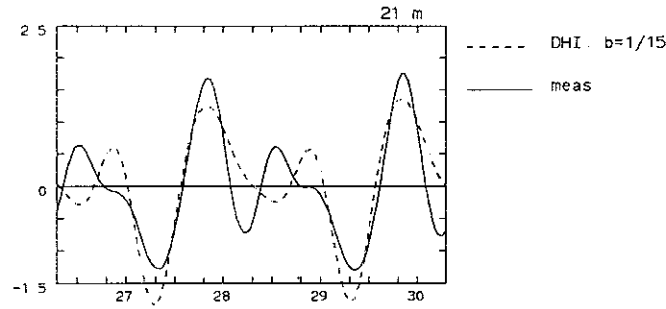


FIG. 12. Comparison DHI, $b = 1/15$, with measurement at $x = 21$ m, case A

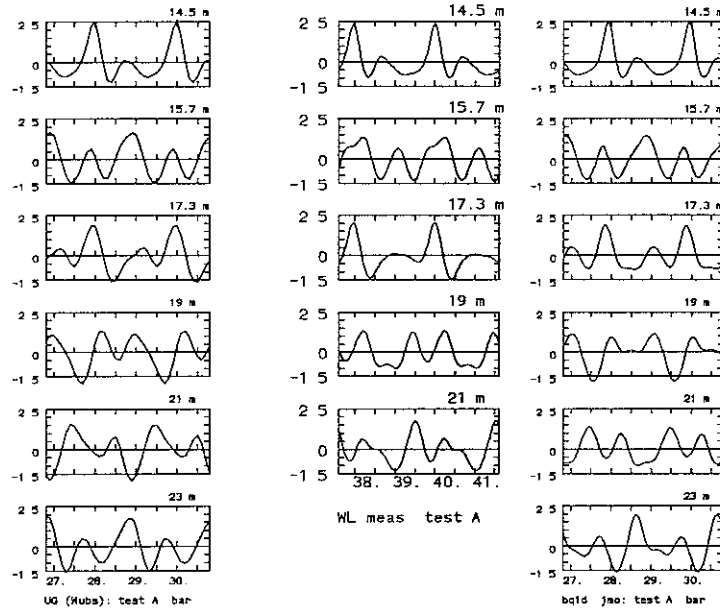


FIG. 13. Results of University of Groningen (left), measurements (middle) and results of Delft Hydraulics (right), test A.

made, has been proposed by Radder (1992). A description of the model and its numerical evaluation in two ways³ is given in Otta and Dingemans (1994). Results from the time-domain model are given in Figure 14, again for stations from 14.5 m onwards. The form as used here is of Boussinesq-type of approximation with respect to the non-linearity but has exact linear dispersion relation. (In the limit for vanishing amplitude the model is the usual linear wave propagation model.) Higher-order approximations with respect to the non-linearity are possible but are not used here. These higher-order non-linearities are short-wave non-linearities. These are of importance, amongst others, in accurate modelling of solitary waves where steep gradients occur.

Because boundary-element models can give an accurate description of the free surface elevation, also a computation has been performed by Broeze with the model Hypan as described by Broeze (1993). These results are also shown in Figure 14.

It is seen that up to 17.3 an excellent correspondence with the measurements is found. Also at 21 m a good correspondence is found, especially for the boundary element model. The Hamiltonian model performs slightly less. This is ascribed to

³ One of the models is the solution of the time-evolution equations. The other one consists of an expansion in terms of sinc functions. Results of the second one are given here.

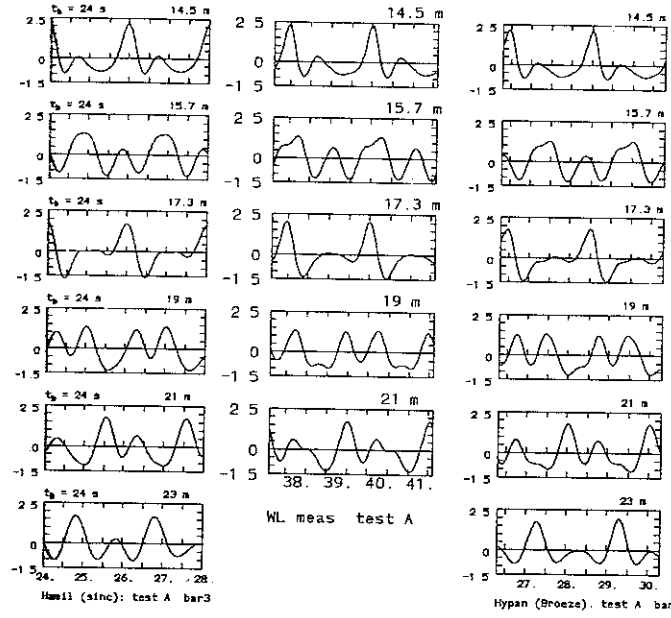


FIG. 14 A Hamiltonian model (left), measurements (middle) and the Hypan model of Broeze (right), test A.

the neglect of the short-wave non-linearities. Notice that the small depression in the crest of the measured free surface profile at 15.7 m is only predicted by the boundary element model. All other computations miss this feature.

At 19.3 m the two peaks in the computed free surface profile are almost equal, as in the measurement, but the phases of the short waves are different. Again it is seen that in the boundary element model more short wave behaviour is visible than in the Hamiltonian model. This is typically due to a better modelling of the non-linearities. We notice that also with Boussinesq (e.g., the DHI model with $b = 1/15$), the correspondence at 19 m was less than the correspondence at 21 m. Possibly this is due to the place in the wave profile where the higher harmonics manifest themselves. When they are visible in the trough a small deviation looks much more significant than when the same deviation occurs elsewhere in the profile.

We conclude that the correspondence between the free surface profiles of the boundary element computation and the measurements is excellent. The Hamiltonian model performs slightly less, but is still slightly better than any of the Boussinesq-type or Serre-type models. This is to be expected because of the correct frequency dispersion in the model.

4.1.4. Legi results.

Legi results are available for the Serre-type model (16)-(19) with two choices for the frequency-dispersion parameter: $B = 0$ and $B = 1/20$. Again only the results at the stations from 14.5 m onwards have been shown, see Figure 15. For $B = 0$ (not so good frequency dispersion) the computed wave profiles differ much with the measured ones, as has been noted before with other models with non-optimal frequency dispersion. For the case $B = 1/20$, as shown in the right-hand side of Figure 15, the correspondence with the measurements is much less than has been obtained for other models with good frequency behaviour, i.e., the DHI model and the two Hamiltonian models (Delft Hydraulics and University of Groningen).

The waves between 28 and 32 s are stable, i.e., all higher-harmonic components

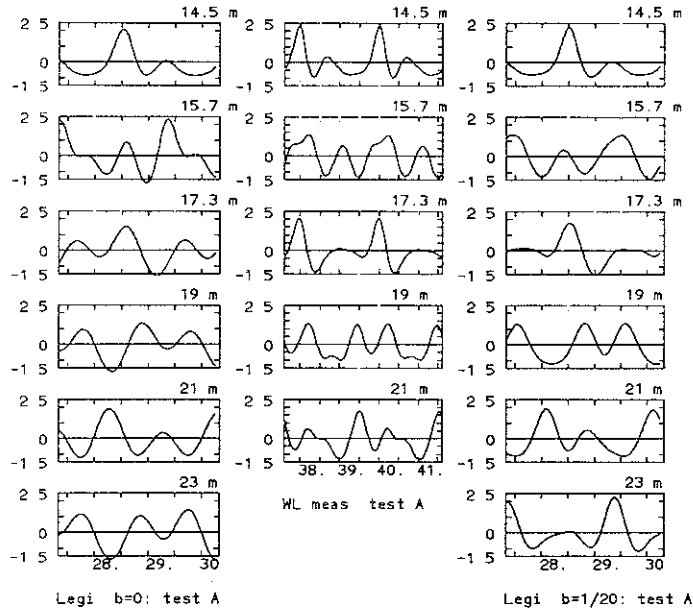


FIG 15. Serre model of Legi. $B = 0$ (left), measurements (middle) and $B = 1/20$ (right), test A

have reached the stations. This is shown in Figure 16 where the full computation between 10 and 40 s has been shown for the stations from 14.5 m onwards.

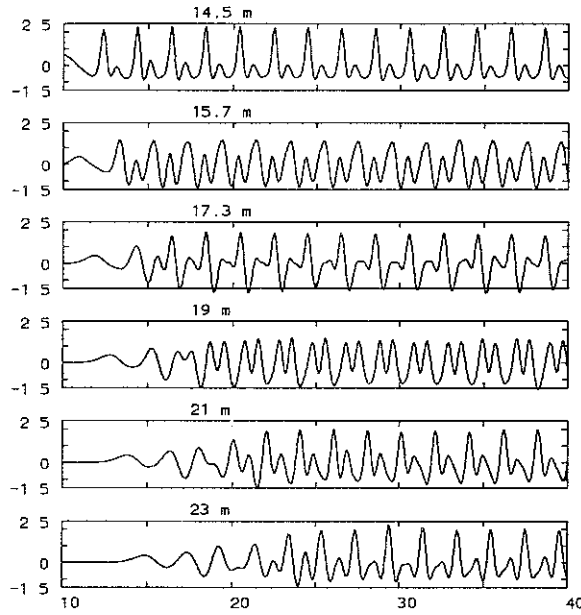


FIG 16 Serre model of Legi. $B = 1/20$ time-window from 10 to 40 s. Test A

This case for Serre thus performs evidently less than the corresponding Boussinesq case for improved frequency behaviour (i.e., the DHI result). This could be the case because $B = 1/20$ is not a Padé expansion of the true linear phase velocity and therefore performs less for small values of kh . This has to be investigated further.

4.1.5. Snamprogetti results.

Snamprogetti furnished computations with both a Boussinesq model and a Serre-type model. The Boussinesq model is given by Eqs. (6). In neither of the models an improved-frequency dispersion formulation has been used. The results have been shown in Figure 17. Because the frequency dispersion is not so good, the computed

free surface profiles behind the bar do not conform well with the measurements. This is already clear from the profiles at 15.7 m, on the backward slope. Some difference between the Boussinesq and the Serre cases is found at the stations 21 and 23 m, but these differences are not large. It is as if the Boussinesq case has different shoaling behaviour because all harmonics are more pronounced in the Boussinesq case than they are in the Serre case. The effect of the shoaling is already visible in the main peak at the station 14.5 m.

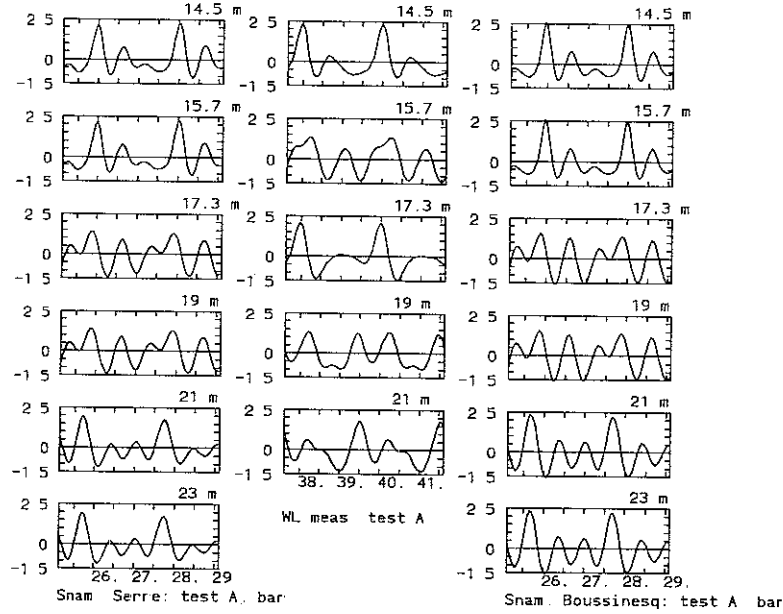


FIG 17 *Snamprogetti: Serre (left), measurements (middle) and Boussinesq (right), test A.*

4.1.6. University of Thessaloniki results.

Aristotle University of Technology (Karambas) furnished computations carried out with different models. One concerns computations with the usual Boussinesq-type model written in the vertically averaged velocity and the second one concerns a Boussinesq-type model with a kind of improved frequency dispersion. Of both models the wave profiles of the stations from 14.5 m onwards are plotted together with the measurements in Figure 18. As could have been expected, the model without frequency-dispersion improvement does not perform so good. The model with frequency dispersion improvement, (the right column in Figure 18) performs very well. At 15.7 and 17.3 m the correspondence with the measurements seems as good as the DHI model (see Figure 10), but at 19 m the DHI model performs slightly better. Both models have essentially the same error at the latter station, which is most clearly seen in the trough of the waves. In the measurement a higher-harmonic is in anti-phase with the basic wave, but in both computations that higher harmonic seems to be in phase with the basic wave. At 21 m the AUT model performs better than the DHI model.

4.2. Measuring condition B.

Results of all models have been shown for measuring condition A. For measuring conditions B and C we now only show results obtained with Boussinesq and Serre models which gave good results for measuring condition A. We now have a longer wave than in case A, which is also evident from the value of the shallowness pa-

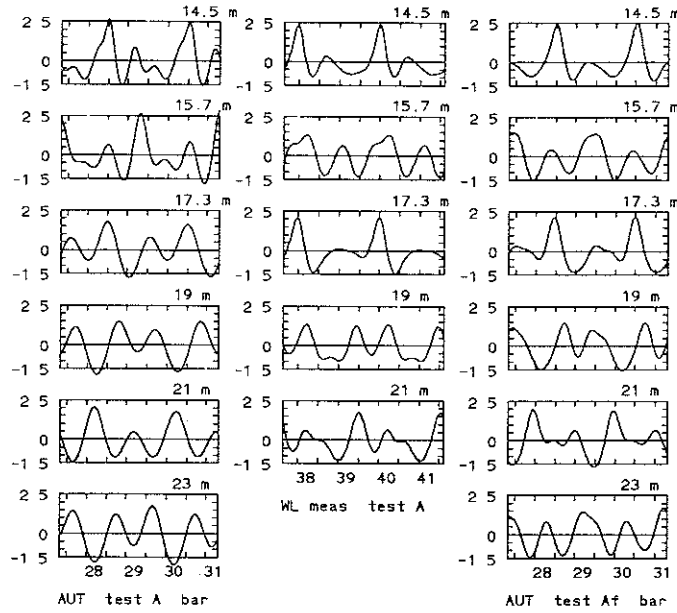


FIG. 18 *AUT*; model (11) (left), measurements (middle) and Boussinesq (right), test A.

parameter $T\sqrt{g/h} = 12.5$. The effect of a longer basic wave is that the generation of higher-harmonics develops stronger (the phase mismatch is smaller and therefore the interaction time that waves may effectively interact with each other is longer). Stronger interaction also means that still higher harmonics may be generated.

We show the results obtained with the Boussinesq model of DHI and the Serre model of Legi. In order to show that a good dispersion relation remains important also for test cases B and C, results with both $b = 0$ and $b = 1/15$ are shown for DHI (Figure 19) and results for both $b = 0$ and $b = 1/20$ are shown for Legi (Figure 20).

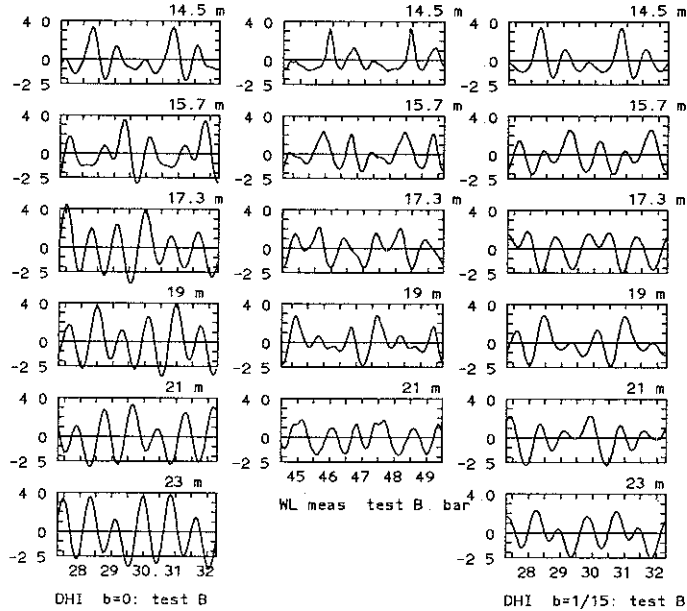


FIG. 19. DHI, Results for $b = 0$ (left) and $b = 1/15$ (right), and measurements (middle), case B; stations from 14.5 m onwards

Consider the right-hand column of Figure 19. A good correspondence is obtained at the station at 14.5 m. At 15.7 m the correspondence between computation and

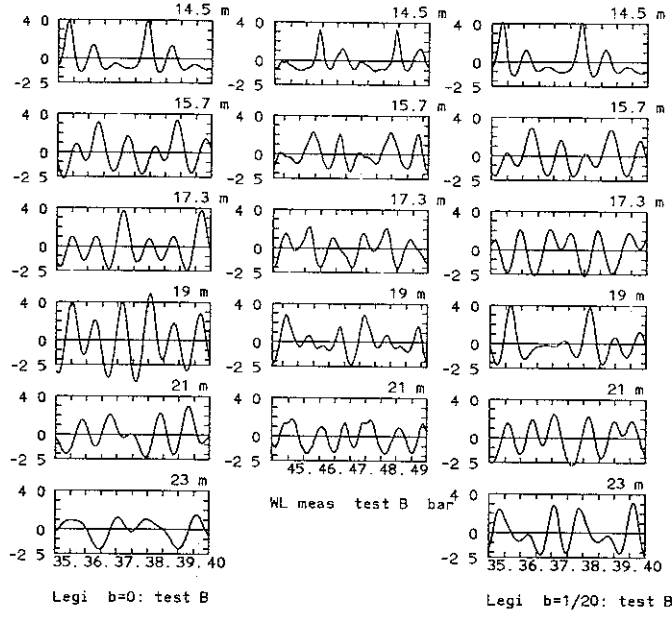


FIG. 20. *Legi*, Results of the Serre model with $B = 0$ (left) and $B = 1/20$ (right), and measurements (middle), case B; stations from 14.5 m onwards.

measurement is much less. In the measurement we have two peaks of approximately equal height between two very small peaks. In the computation these two peaks are of unequal height. The correspondence at 17.3 and 19 m seems to be better than that at 15.7 m.

4.3. Measuring condition C.

For measuring condition C we show the results of DHI for both $b = 0$ and $b = 1/15$ (Figure 21) and the ones of the Serre model of *Legi* with $b = 0$ and $b = 1/20$ (Figure 22). For this condition we have $T\sqrt{g/h} = 5.0$ in the deep part, so we have a rather short basic wave. Whereas the measured free surface profiles are tilted first to the right, and later to the left, the computed profiles, especially from 15.7 m onwards are very symmetrical with respect to the vertical. It is as if the computations are not able to generate enough second and third harmonic amplitude. As for the generation of higher harmonics a small phase mismatch (i.e., $\Delta k - k_2 - 2k_1$) is permitted, the mismatch grows rapidly for shorter waves, and, moreover the error between the mismatch as experienced in the Boussinesq model and the one in the measurements also grows. Therefore, in the measurements a smaller mismatch would be present with as effect more higher-harmonic constituents in the signal.

The result from both the Boussinesq-type model and the Serre-type model, both with improved frequency dispersion, is very disappointing. For the *Legi* model without frequency dispersion improvement the results at 21 and 23 m are strange. This needs further attention. We therefore plot all the computational data beyond 10 s, see Figure 23. For $B = 0$ 10 s the computation time is shorter than for the case $B = 1/20$. In fact 40 s is needed.

5. Discussion and recommendations.

We see that it is important that the free harmonics have an accurate phase velocity. The frequency-dispersion modelling is much more important than the modelling for possible higher waves. Thus the competition between Serre-type and Boussinesq-

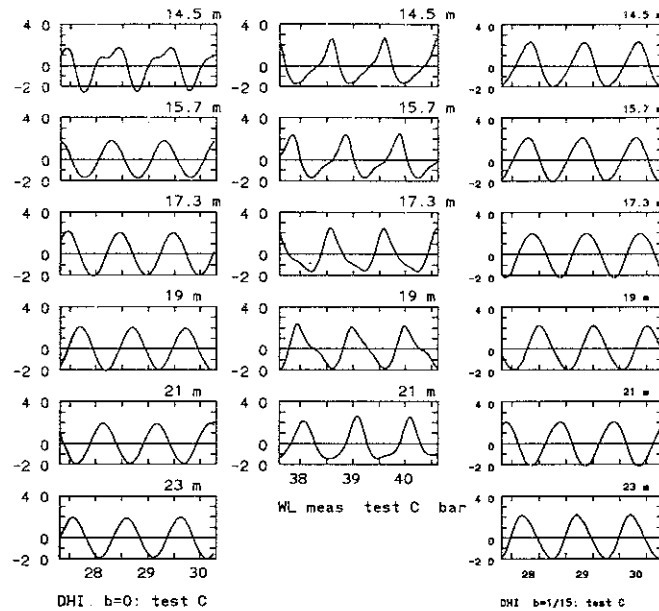


FIG 21. DHI, Results for $b = 0$ (left) and $b = 1/15$ (right), and measurements (middle), case C; stations from 14.5 m onwards.

type models is won by the one with best frequency dispersion characteristics. That is, the linear properties are the most important ones for good correspondence with measurements. Of course, that does not mean that no modelling of non-linearity is necessary, because the non-linearity is the source of the generation of higher harmonics, and these higher harmonics, when they get free, have their own phase velocity. In (fairly) long-wave approximations the attention is usually focussed to the basic wave to be long enough, but also the third or fourth harmonic should have a wave length which is long enough.

For models with the same frequency behaviour the differences are in the modelling of the nonlinearity and the modelling of the slope-dependent terms. For small slopes, Madsen et al. (1992) have shown that small differences in the depth-dependent terms may give large differences in the linear shoaling characteristics. A number of examples with widely different shoaling characteristics have been discussed also by Dingemans (1984).

The Boussinesq-type and Serre-type models of DHI and Legi-IMG do not perform well for test C. This needs further investigation. Although the results of the other models have not been shown, we have no reason to believe that these would perform essentially better for test C. In first instance it would be useful to see whether a good model such as the boundary-element model HYPAN of Broeze performs well for this situation. Perhaps the Hamiltonian model would also be accurate enough, it certainly is easier to run than the boundary-element model.

Lastly it should be mentioned that none of the various investigators who made results of their computations available had access to the measurements. The measurements are to be distributed after completion of this note

Acknowledgement This work was undertaken as part of the MAST G8M Coastal Morphodynamics research programme. It was funded jointly by Delft Hydraulics and by the Commission of the European Communities, Directorate General for Science, Research and Development, under MAST contract no. MAS2-CT92-0027.

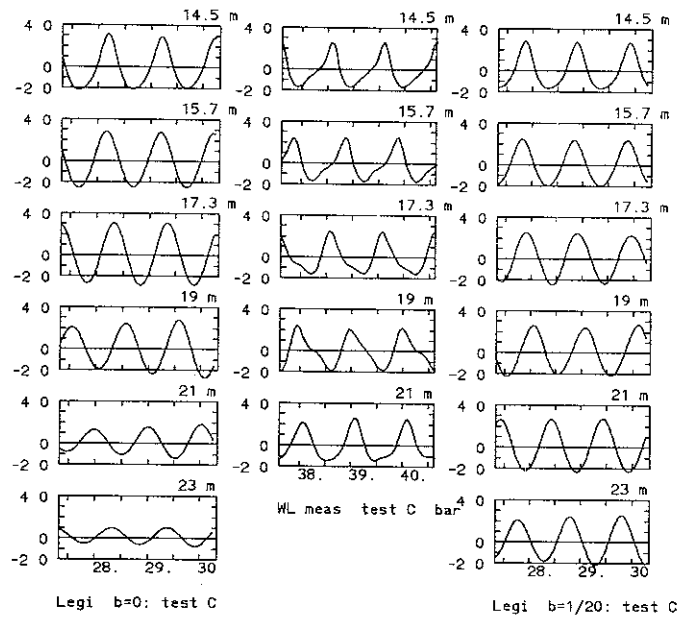


FIG. 22. *Legi*, Results the Serre model with $B = 0$ (left) and $B = 1/20$ (right), and measurements (middle); stations from 14.5 m onwards, case C

Part of the work has been carried out while the author worked at the International Centre for Computational Hydrodynamics in Denmark and has been funded by the Danish National Science Foundation. The author wishes to express his gratitude to Gert Klopman of Delft Hydraulics for making available a new set of experiments which form the basis for the present intercomparison study. This study would not have been possible without the help of the various investigators who made available the results of their computations.

REFERENCES

- [1] Beji, S. and Battjes, J.A., 1993. Experimental investigations of wave propagation over a bar. *Coastal Engineering* **19**(1,2), pp. 151-162.
- [2] Broeze, J., 1993. Numerical modelling of nonlinear free surface waves with a 3D panel method. *Thesis Techn. Univ. Twente*, 228 pp.
- [3] Dingemans, M.W., 1973. Water waves over an uneven bottom; a discussion of long-wave equations. *Delft Hydraulics*, Report R729 part 2, 88 pp.
- [4] Dingemans, M.W., 1973. Water waves over an uneven bottom; a discussion of long-wave equations. *Delft Hydraulics*, Report R729 part 2, 88 pp.
- [5] Dingemans, M.W., 1976a. Water waves over an uneven bottom; some numerical experiments. *Delft Hydraulics*, Report R729 part 5, 63 pp.
- [6] Dingemans, M.W., 1987. Verification of numerical wave propagation models with laboratory measurements; HISWA verification in the directional wave basin. *Delft Hydraulics*, Report H228, part 1, 400 pp.
- [7] Dingemans, M.W. (1994). *Water Wave Propagation Over Uneven Bottoms*. World Scientific, Singapore, to be published.
- [8] Madsen, P.A., Murray, R. and Sørensen, O.R., 1991. A new form of the Boussinesq equations with improved linear dispersion characteristics. *Coastal Engineering* **15**(4), pp. 371-388.
- [9] Madsen, P.A. and Sørensen, O.R., 1992. A new form of the Boussinesq equations with improved linear dispersion characteristics. Part 2: A slowly-varying bathymetry.

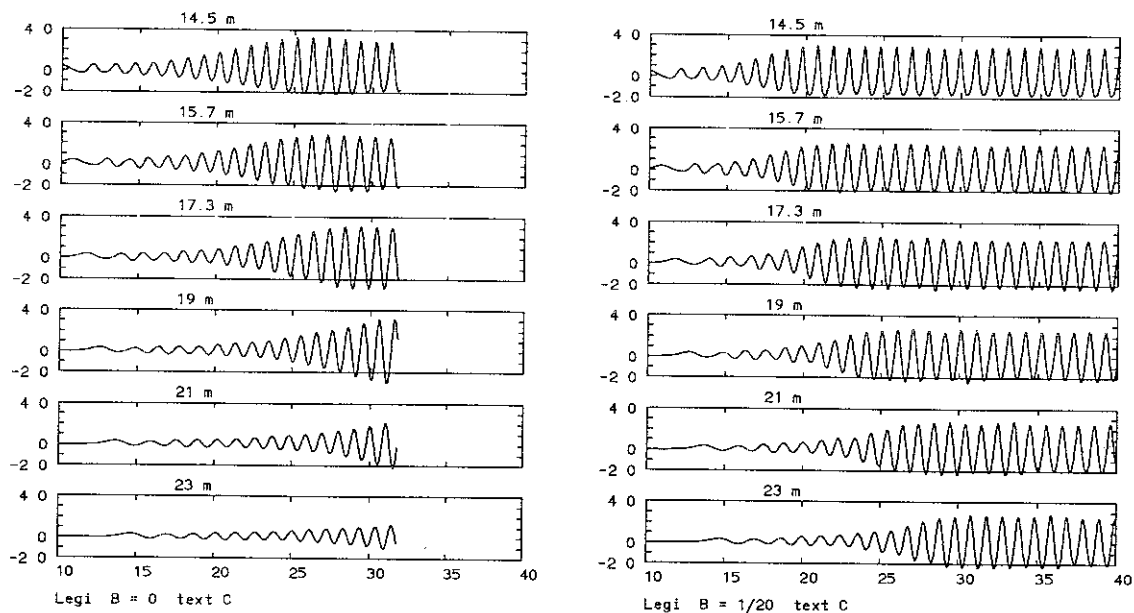


FIG 23. Serre model of Legi. Test C. left $B = 0$ and right $B = 1/20$ time-window from 10 to 40 s.

Ocean Engineering 18(3/4), pp. 183-204.

- [10] Liberatore, G. and Petti, M., 1992 Wave transformations over a submerged bar: experiments and theoretical interpretations. *23rd Proc. Coastal Engng Conf.*, Venice, Vol. 1 pp. 447-459
- [11] Luth, H.R, Klopman, G. and Kitou, N., 1994. Project 13G: Kinematics of waves breaking partially on an offshore bar; LDV measurements for waves with and without a net onshore current. *Delft Hydraulics Report H1573*, March 1994, 40 pp.
- [12] Mooiman, J., 1991. Boussinesq equations based on a positive definite Hamiltonian. *Delft Hydraulics Report Z294*, 78 pp.
- [13] Otta, A.K. and Dingemans, M.W. (1994) Hamiltonian formulation of water waves; formulation, numerical evaluations and examples. *Delft Hydraulics Report H782*, May 1994, approx. 70 pp.
- [14] Radder, A. C. (1992). An explicit Hamiltonian formulation of surface waves in water of finite depth. *J. Fluid Mech.* 237:435-455.
- [15] Su, C.H. and Mirie, R.M., 1980. On head-on collisions between two solitary waves. *J. Fluid Mechanics* 98, pp. 509-525.
- [16] Veen, W.A. Van der, and Wubs, F.W., 1993. A Hamiltonian approach to fairly low and fairly long gravity waves. Report **W-9314** *Department of Mathematics, Univ. of Groningen*, 25 pp.
- [17] Witting, J.M., 1984. A unified model for the evolution of nonlinear water waves. *J. of Computational Physics* 56(2), pp. 203-236

